Journal of Power Sources 261 (2014) 238–244

Contents lists available at ScienceDirect

Journal of Power Sources

journal homepage: www.elsevier.com/locate/jpowsour

Nitrogen-rich mesoporous carbon derived from melamine with high electrocatalytic performance for oxygen reduction reaction

Rongfang Wang [a,*], Tiaobao Zhou [a], Hao Li [b], Hui Wang [a], Hanqing Feng [c], Jonathan Goh [d], Shan Ji [d,**]

[a] Key Laboratory of Eco-Environment-Related Polymer Materials, Ministry of Education of China, College of Chemistry and Chemical Engineering, Northwest Normal University, 967 Anning East Road, Lanzhou, Gansu 730070, China
[b] Department of Chemical Engineering, Huizhou University, Huizhou, Guangdong 516007, China
[c] College of Life Science, Northwest Normal University, Lanzhou 730070, China
[d] South African Institute for Advanced Materials Chemistry, University of the Western Cape, Private Bag X17, Bellville 7535, Cape Town, South Africa

HIGHLIGHTS

- Nitrogen-rich mesoporous carbon derived from melamine (MNMC) is prepared.
- MNMC shows good catalytic activity for oxygen reduction reaction.
- The good performance is derived the special structure.

GRAPHICAL ABSTRACT

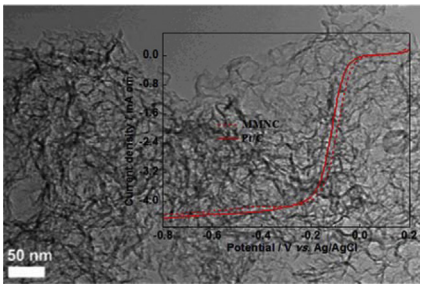

ARTICLE INFO

Article history:
Received 29 December 2013
Received in revised form
7 March 2014
Accepted 17 March 2014
Available online 25 March 2014

Keywords:
Mesopore
Nitrogen-rich carbon
Electrocatalyst
Oxygen reduction reaction

ABSTRACT

Melamine-derived N-doped mesoporous carbon (MNMC) is synthesized by the pyrolysis of lysine and melamineunder at nitrogen atmosphere using ferric chloride as a dopant and SiO_2 nanoparticles as hard templates to form mesoporous architecture. The N content in the bulk of carbon materials is as high as 11.3% and ca. 40.6% of N is in the form of pyridinic-N. The surface area of MNMC is ca. 650 m^2 g^{-1} with a pore size distribution in the range of 2.2–34.5 nm. Compared to commercial Pt/C (20 wt%), MNMC exhibits much better electrocatalytic activity, better durability, and higher methanol tolerance for oxygen reduction reaction (ORR) in alkaline medium. Particularly, the onset ORR potential and half-wave ORR potential of MNMC are 1.059 and 0.871 V *vs.* RHE respectively, which are higher than those of commercial Pt/C.

1. Introduction

Slow kinetics characteristic of the cathodic oxygen reduction reaction is one of the primary limitations for the commercialization of fuel cells [1–3]. To date, platinum based catalysts are still the best cathodic materials for the oxygen reduction reaction (ORR) and are widely used in commercial fuel cells. However, the high cost, low durability, as well as the slow reduction kinetics of Pt-based

* Corresponding author. Tel./fax: +86 931 7971533.
** Corresponding author. Tel./fax: +27 21 9599316.
E-mail addresses: wrf38745779@126.com, wangrf@nwnu.edu.cn (R. Wang), sji@uwc.ac.za (S. Ji).

http://dx.doi.org/10.1016/j.jpowsour.2014.03.057
0378-7753/

catalysts hinder the large-scale application of fuel cells. Many efforts have been made to reduce the cost of cathodic catalysts by two approaches [4]: (1) reducing the Pt loading by increasing Pt utilization in the catalyst layers [5–7]; (2) replacing Pt with noble-metal-free catalysts [8–11]. Among these catalysts, nitrogen-doped (N-doped) carbon has been demonstrated to be a promising alternative to Pt-based catalysts for fuel cells.

Carbon materials are widely used as support materials for Pt-based catalysts due to their porous structure, high electrical conductivity and stability [12,13]. In particular, the carbon materials with mesoporous structures have attracted a lot of attention on account of their large surface area and mesoporous network, which improve the transport of educts and products formed on the surface of catalysts, thereby increasing the performance of the catalysts and lowering the total cost of fuel cell systems [14,15]. The electrochemical properties of mesoporous carbon can be significantly enhanced by introducing heteroatoms, such as N, into its structure [16,17]. After introducing electron-rich nitrogen atoms into carbon materials, the π electrons in carbon materials can be activated due to the lone-pair electron from N [18]. There are two common routes to obtained N-doped carbon materials. The first one is to treat the pre-synthesized carbon materials with N-containing materials, such as NH_3. The other one is to directly pyrolyze N-contained carbon materials, which is a one-step process. In general, N-doped carbon materials prepared via. the second route will have higher N content compared with those prepared via. the first route.

It has been reported that there are four types of nitrogen species in carbon-based materials including pyridinic-N, pyrrolic-N, quaternary nitrogen, and pyridinic N^+-O^-, respectively [19]. Pyridinic-N can provide one *p*-electron to the aromatic π-systems, which has a pair of electrons in the plane of the carbon matrix. So pyridinic-N can increase the electron-donor property of the catalyst and thus enhance the electrocatalytic activity of N-doped carbon materials [20]. Usually, nitrogen containing polymers such as polypyrrole [21], polyvinylpyrrolidone [22], and polyaniline [23], were used as precursors to prepare N-doped mesoporous carbons. Unfortunately, in most cases, these polymers were not rich of pyridinic-N and the resulted N-doped carbon did not show higher performance for ORR than commercial Pt/C catalyst in term of both activity and stability. It is expected that mesoporous carbon materials with high pyridinic-N content is highly desirable, which are expected to exhibit high performance for ORR.

It is well known that melamine is a type of three triazine heterocyclic organic compound with high pyridine-N content [24]. In this work, an effective method was developed to prepare melamine-derived N-doped mesoporous carbon (MNMC) with high pyridinic-N content by temperature-programmed thermal pyrolyzing lysine and iron modified melamine in a nitrogen atmosphere with ferric chloride as an activator and SiO_2 nanoparticles as templates to form a porous structure. A schematic illustration of this method is shown in Fig. 1. The as-prepared MNMC were characterized by means of X-ray photoeletron spectroscopy, scanning electron microscopy, transmission electron microscopy, as well as Raman spectroscopy. The electrochemical tests demonstrated that MNMC exhibits higher electrocatalytic activity and stability towards ORR than the commercial Pt/C catalyst.

2. Experimental

2.1. Preparation of MNMC

4.48 g melamine and 0.52 g lysine were dissolved into a $FeCl_3$ (0.25 g) methanol/water solution ($V_{methanol}$:V_{water} = 0.5), and the mixture was then stirred magnetically and ultrasonicated for 1 h at room temperature. 1.0 g SiO_2 nanoparticles (ca. 30 ± 15 nm, Aladdin) was added to the above mixture under stirring and then ultrasonicated to obtain homogeneity. The obtained mixture was dried at 80 °C in a vacuum oven overnight. After the resulted powder was heated at 300 °C for 1 h in nitrogen atmosphere, the temperature was elevated to 900 °C at the rate of 5 °C min^{-1} under nitrogen flow and that temperature was maintained for 1 h. In order to remove SiO_2 template, The as-obtained powder was immersed in HF (20 wt%, 6 mL) solution under stirring for 24 h, and

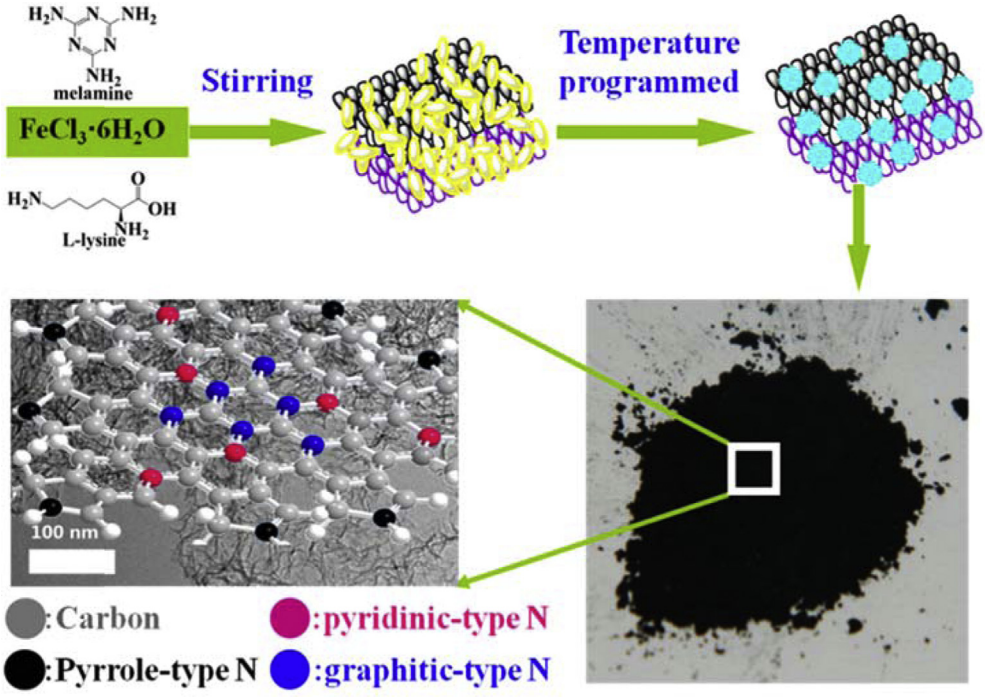

Fig. 1. Schematic route of preparation of MNMC.

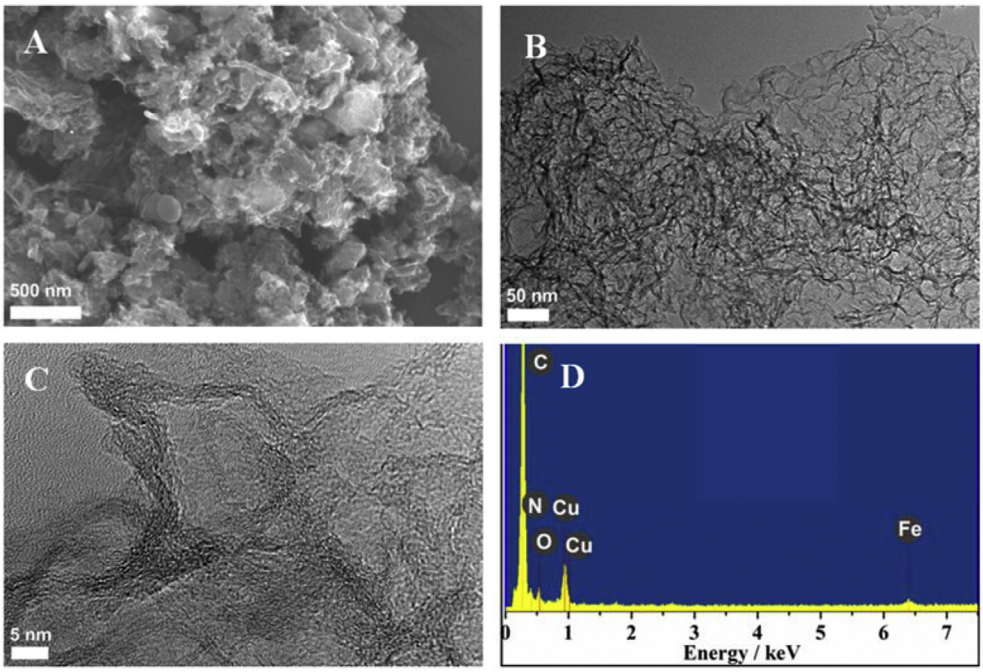

Fig. 2. SEM (A), TEM (B) and HRTEM (C) images of MNMC; EDX (D) images of MNMC.

then washed for 10 times with ultrapure water. The powder was collected by centrifugation and dried at 60 °C.

For comparison, carbonized lysine (L) was prepared by heat-treating lysine at 900 °C in a nitrogen atmosphere; a mixture of melamine and lysine, and a mixture of melamine, lysine and $FeCl_3$ were also carbonized at 900 °C to prepare carbonized melamine and lysine (M + L), carbonized melamine, lysine and $FeCl_3$ (M + L + Fe); carbonized melamine with $FeCl_3$ (M + Fe) as an activator was synthesized by pyrolyzing melamine and $FeCl_3$ at 900 °C.

2.2. Physical characterization

Elemental analysis was performed using an organic elemental analyzer, Thermo Flash 2000. X-ray photoeletron spectroscopy (XPS) was obtained on a VGEscalab210 Spectrometer fitted with Mg 300 W X-ray source (England). Scanning electron microscope (SEM) measurements were carried out on a Carl Zeiss Ultra Plus (Germany). Transmission electron microscopy (TEM) was carried out on a JEM-2010 Electron Microscope (Japan) with the acceleration voltage of 200 kV, coupled with energy dispersive X-ray analysis (EDX). Raman spectroscopy measurements were carried out on Ft-Raman spectroscopy (RFS 100, BRU-KER) employing Nd: YAG laser wavelength of 1064 nm. The specific surface area was determined by Brunauer–Emmett–Teller (BET) method and the pore size distribution (PSD) was calculated by the density functional theory (DFT) method. Elemental Analysis was measured by Organic Elemental Analyzer (Thermo Flash2000).

2.3. Electrochemical characterization

The activity for ORR was evaluated on an Autolab electrochemical work station (Netherlands, Autolab, PGSTAT128N). A conventional constant temperature three-electrode cell was used, including an Ag/AgCl (saturated KCl) electrode as the reference electrode, a platinum wire as the counter electrode, and a glassy carbon-rotating disk electrode (GC-RDE) as the working electrode. The thin-film electrode was prepared as follows: 5 mg of MNMC was dispersed ultrasonically in 1 mL Nafion/ethanol (0.25% Nafion) solution for 5 min. 8 μL suspensions dropped on the surface of the

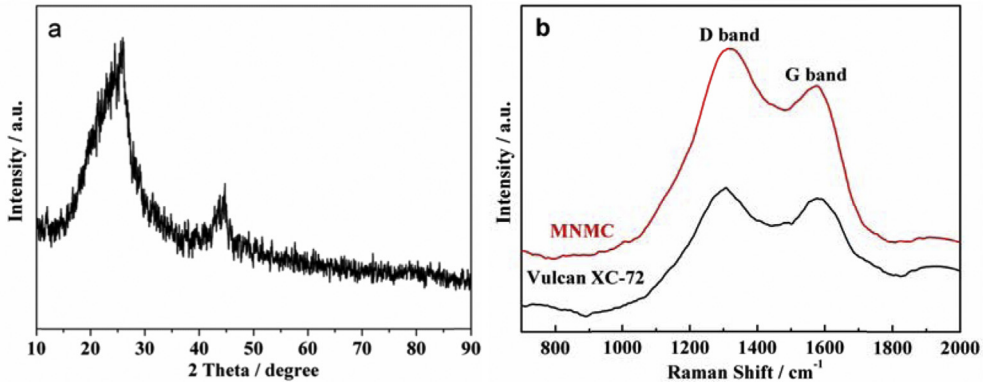

Fig. 3. (a) XRD pattern of MNMC; (b) Raman spectra of the MNMC and Vulcan XC-72 Carbon.

glassy carbon rotating disk electrode, followed by drying in air at room temperature. For comparison, a commercially available Pt/C (20 wt% J. M. Corp.) was prepared similarly on the GC-RDE. The characterization of commercial Pt/C such as XRD, TEM was provided in Supporting Information. The electrocatalyst loading on the electrode is 0.04 mg cm^{-2}. All potentials initially measured versus the Ag/AgCl electrode were converted to an RHE scale by adding 0.966 V (the potential of the Ag/AgCl reference measured against RHE).

3. Results and discussion

The morphology and structure of MNMC were studied by SEM and TEM, and the results are shown in Fig. 2. It can be seen in Fig. 2(A) that a three-dimensional (3D) porous structure is formed. In the TEM image of MNMC (Fig. 2(B)), irregularly sheet-like carbon with numerous mesopores is observed, on which the pore size is similar to the particle size of SiO_2 template. The results indicate that it is feasible to synthesize mesoporous N-doped carbon using silica spheres as a hard template. The high resolution magnified image (HRTEM) in Fig. 2(C) shows that the material exhibits stacking graphite layers, indicating the formation of the grphite structure in MNMC. The EDX result of MNMC in Fig. 2(D) shows that nitrogen, oxygen and iron elements are detected in MNMC.

The XRD pattern of MNMC is shown in Fig. 3(a). Three diffraction peaks at 25.2°, and 44.3°are attributed to the (002) and (101) peaks of hexagonal graphite structures, suggesting coke-like structural features with disordered carbonaceous interlayers [25,26]. Raman spectroscopy was carried out to investigate the chemical structure and the degree of structural defects of MNMC. Fig. 3(b) shows the Raman spectrum of MNMC. For comparison, that of Vulcan XC-72 carbon is also presented. It is found that both samples showed two peaks at 1305–1320 and 1575–1581 cm^{-1}, corresponding to Raman active D- and G-band respectively [27]. The Raman D-band originates from atomic displacement and disorder induced features caused by lattice defects and distortions, while the G-band results from the in-plane vibration of E_{2g} phonon of sp^2-bonded carbon atoms [2]. The relative intensity (I_D/I_G) ratio was widely used to estimate the amount of defects on N-doped carbon [28]. The I_D/I_G ratios of MNMC and Vulcan XC-72 carbon are 1.2 and 1.1 respectively. The I_D/I_G of MNMC is higher than that of Vulcan XC-72 carbon, indicating that MNMC has more defects than Vulcan XC-72 carbon. As expected, introducing N atoms into carbon will result in an increase in the relative intensity of D-band due to the increase of defects caused by N atoms [29].

XPS was conducted to investigate the surface composition and the chemical state of MNMC (Fig. 4(A) and (B)). As shown in Fig. 4(A), the survey spectrum of MNMC confirms that there is carbon (C1s = 284.8 eV), nitrogen (N1s = 399.1 eV), and oxygen (O1s = 532.3 eV) in MNMC. The absence of characteristic peaks of Fe at 705–730 eV in the XPS survey spectrum indicates that no element of iron is detected on the surface of MNMC, which doesn't agree with the EDX results. The above results suggest that the iron previously on the surface of MNMC is completely removed during the post-treatment processes and only exists in the bulk of MNMC.

Table 1
The atomic ratio of nitrogen species in MMNC derived from N 1s XPS spectrum and the nitrogen content of bulk M + Fe, M + L, M + L + Fe, and M + L + Fe + SiO_2 obtained by element analysis.

Sample		MNMC	
Nitrogen species	Pyridinic-N	Pyrrolic-N	Graphitic-N
Atomic content (%)	40.7	22.3	37.0
Sample	M + Fe	M + L + Fe	MNMC
Nitrogen content (wt %)	6.6	11.9	11.3

The N 1s spectrum is very useful for analyzing the nature of N functionalities on MNMC. Fig. 4(B) shows high resolution N 1s spectrum of MNMC, which can be deconvoluted into three dominant peaks, which are assigned to pyridinic-type N (398.5 eV), pyrrolic-type N (399.8 eV), and graphitic-type N (400.7 eV), respectively [19]. Results of Quantitative analysis of the N 1s spectrum of MNMC showed in Table 1 reveal that the amount of pyridinic-type N accounts for 40.7% of nitrogen species, which plays a key role in improving the catalytic ORR activity. Pyridinic-type N bonded with two edge carbon atoms has one lone pair of electrons which can facilitate the electron transfer and the adsorption of oxygen, and further results in enhanced ORR activity. The content of nitrogen in the bulk of MNMC by elemental analysis is 11.3 wt%, showing that MNMC is a nitrogen rich carbon material. To our knowledge, the highest value of nitrogen content, 13.6 wt%, was reported by Lu's group through post-functionalization [30]. For a one-step synthesis of N-doped carbon, the highest value of ca.12 wt % was obtained in the work of Yang et al. [31], who used the composite precursors of 1-ethyl-3-methaylimidazolium dicyanamide ionic liquid and adenine. As we known, the carbon materials with high N content, particularly pyridinic-N, would have high catalytic activity for ORR [32,33]. This value for MNMC is significantly higher than the results of N-doped cathode catalysts [32–34], implying that MNMC would exhibit high catalytic activity for ORR. A comparison of carbon materials derived from melamine with different precursors in Table 1 suggests that the high nitrogen content in MNMC is related to the addition of lysine.

Fig. 5 shows the nitrogen adsorption–desorption isotherms and PSD of MNMC. The nitrogen isotherm curve is a typical type curve with an H3-type of hysteresis loop (International Union of Pure and

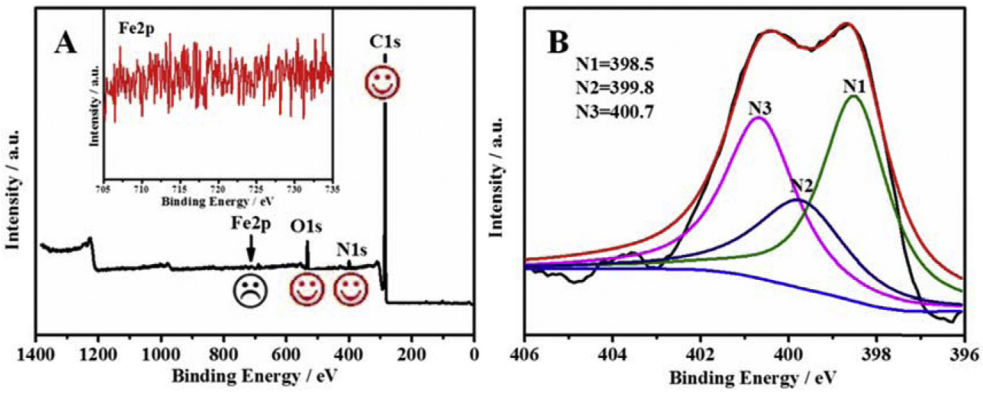

Fig. 4. (A) XPS survey spectrum and (B) deconvoluted N1s XPS spectrum of MNMC.

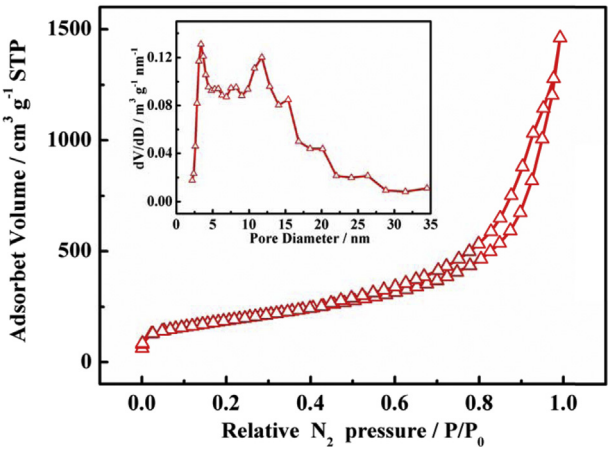

Fig. 5. Nitrogen isotherms and (Inset) the corresponding pore size distribution of MNMC.

Applied Chemistry). This means that the MNMC is a mesoporous and/or large-mesoporous material [28]. PSD of MNMC in the range of 2.2–34.5 nm shown as the inset in Fig. 5 is mainly centered at ca. 3.4 and 11.7 nm, demonstrating that MNMC is a large-mesoporous material. Besides, it is also observed that different pore sizes are distributed in the mesoporous range, suggesting the presence of hierarchical mesopores. BET surface area of MNMC is 650 $m^2\ g^{-1}$. These results show that disordered mesoporous structure in MNMC was formed.

Cyclic voltammograms (CV) were measured to investigate the electrochemical performance of MNMC in 0.1 mol L^{-1} KOH aqueous solutions saturated separately with N_2, and O_2-saturated 3 mol L^{-1} CH_3OH at a scan rate of 50 mV s^{-1}. As shown in Fig. 6(A), in N_2-saturated KOH solution, no current peak is observed in the potential range from 0.166 to 1.166 V. In the O_2-saturated KOH solution, a peak at 0.796 V *vs.* RHE is clearly observed in the CV, demonstrating that the MNMC has catalytic activity towards the ORR. When MNMC is tested in 0.1 mol L^{-1} KOH + 3 mol L^{-1} CH_3OH solution which was saturated with O_2, the peak for ORR also clearly appear in the CV. However, the peak characterized of methanol oxidation reaction is not observed, indicating that MNMC is inert for methanol oxidation reaction in KOH solution saturated with O_2. These results show that MNMC possesses not only the catalytic activity for ORR, but also highly tolerant to methanol [3].

The electrocatalytic activities of M + Fe, M + Fe + L, MNMC and commercial Pt/C were studied by linear sweep voltammetry (LSV) in O_2-saturated 0.1 mol L^{-1} KOH aqueous solution (Fig. 6(B)). The curves ranged from 0.9 to 1.2 V shown as the inset in Fig. 6(B) are enlarged to clearly illustrate the occurrence of the ORR on the electrodes. The electrocatalytic activity of MNMC towards the ORR is benchmarked against the activity of commercial Pt/C. In Fig. 6(B), all of the catalysts exhibit a flat plateau and a sharp transition of control from kinetics to diffusion, which implies a one-step, four-electron pathway for the ORR on these electrodes [10]. It can be seen that M + Fe shows electrocatalytic ORR activity. After adding lysine into the precursor, The onset potential and half-wave potential of the resulted sample, M + L + Fe, are shifted positively to 1.03 and 0.852 V respectively, compared with those of M + Fe. The above results could be attributed to the increase of nitrogen content and surface area due to the addition of lysine into the precursor, leading to more active sites which enhanced the catalytic activity for ORR.

In the case of MNMC, the onset potential and half-wave potential are 1.059 V and 0.871 V (see Fig. 6(C)) respectively, indicating better catalytic activity of MNMC for ORR compared to M + L + Fe. The enhanced catalytic activity of MNMC could be attributed to the high pyridine-N content and high surface area. Furthermore, the onset potential and half-wave potential of MNMC

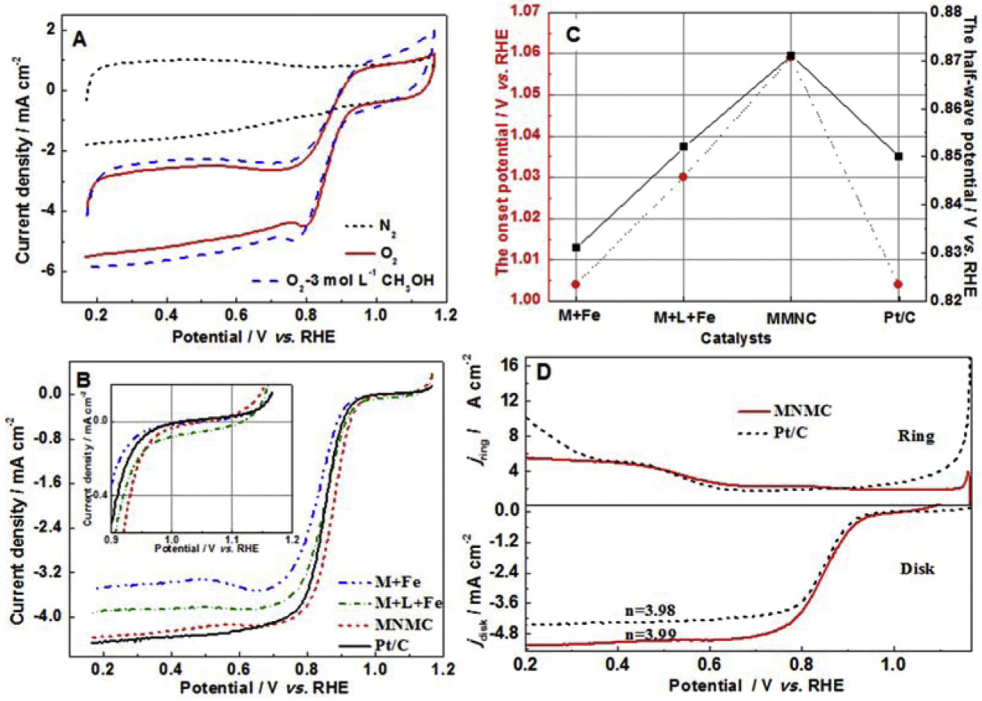

Fig. 6. (A) CVs of MNMC in N_2 or O_2-saturated 0.1 mol L^{-1} KOH and O_2-saturated 0.1 mol L^{-1} KOH and 3 mol L^{-1} CH_3OH solutions at a scan rate of 50 mV s^{-1} and rotation rate of 1600 rpm. (B) LSVs of M + Fe, M + L + Fe, MNMC and Pt/C for ORR in 0.1 moL L^{-1} KOH aqueous solutions at a scan rate of 5 mV s^{-1} and rotation rate of 1600 rpm; The inset: the enlarged region between 0.9 and 1.2 V. (C) The onset potential and half-wave potential of M + Fe, M + L + Fe, MNMC and Pt/C for ORR derived from LSVs in figure B. (D) RRDE response recorded at 5 mV s^{-1} scan rate for MNMC and Pt/C in 0.1 mol L^{-1} KOH solution saturated with O_2 at a rotation rate of 1600 rpm.

are higher than those of commercial Pt/C catalyst (shifted positively about 37.0 mV and 25.0 mV respectively). Compared to other catalysts, the excellent electrocatalytic performance for ORR on MNMC can be attributed to its higher pyridinic-N content and mesoporous architecture, which provide a high density of active sites and plenty of mass diffusion channels for ORR.

The ORR is a multi-electron reaction that has two main possible pathways: one is direct oxidation pathway, involving four electrons transferred to produce water, and its oxidation efficiency is better; the other is indirect oxidation pathway, of which the first stage is two electrons transferred to produce hydrogen peroxide and then the transfer of another two electrons to generate water. the oxidation efficiency of this pathway is relatively low [35]. The ORR mechanism of MNMC was investigated using for rotating ring disk electrode (RRDE) measurements. Fig. 6(D) shows the RRDE voltammograms of MNMC and commercial Pt/C which were carried out in 0.1 mol L^{-1} KOH solution saturated with O_2 at a rotation rate of 1600 rpm. The electron transfer number involved in the ORR can be calculated from following equation [36]:

$$n = 4I_{disk} \Big/ (I_{disk} + I_{ring}/N) \quad (1)$$

where I_{ring} is the Faradaic ring current, I_{disk} is the Faradaic disk current, and N is the collection efficiency, i.e. 0.27. When the disk currents are stabilized after the potential is lower than 0.366 V, n of MNMC and commercial Pt/C are calculated to be 3.99 and 3.98, respectively, indicating ORR mechanism on MNMC is following the four electron pathway.

The methanol crossover effect is a key factor in developing electrocatalysts for direct methanol fuel cells. The methanol crossover effects on MNMC and commercial Pt/C catalysts were investigated by chronoamperometry at a constant voltage of 0.706 V in 0.1 mol L^{-1} KOH solution saturated with O_2 and methanol added at 2000 s (as shown in Fig. 7(A)). It can be seen that there is a shape decrease in current for both MNMC and commercial Pt/C catalysts when O_2 was introduced into N_2-saturated 0.1 mol L^{-1} KOH solution at 1000 s, indicating that the ORR occurs on both catalysts. After methanol is added at 2000 s, there is a sharp current change on commercial Pt/C, which is attributed to the occurrence of methanol oxidation. However, only a slight current change is observed in the ORR current on MNMC after addition of methanol solution. Thus, these results indicate that MNMC possesses a remarkable tolerance to methanol crossover with high selectivity for ORR, which can alleviate the methanol crossover effect occurred in methanol direct fuel cells.

Catalyst stability is another critical feature of ORR electrocatalysts. The stability of MNMC and Pt/C was tested using cycling LSVs in 0.1 mol L^{-1} KOH saturated with O_2. The LSVs of Pt/C and MNMC before and after 10,000 cycles are shown in Fig. 7(B) and (C). The stability can be measured by the decay of half-wave potential before and after a long cycling testing. From Fig. 7(B), it can be seen that the half-wave potential of commercial Pt/C catalyst reduces by 25 mV after 10,000 cycles, but that of MNMC only decreases about 9 mV under the same conditions. Besides, Pt/C lost 10% in current density at 0 V after about 10,000 cycles of potential cycling in Fig. 7(D). However, MNMC exhibited only 1% decrease in current density at 0.966 V. Based on these results, MNMC demonstrates better stability than commercial Pt/C under the same conditions.

4. Conclusions

A high pyridinic-N content and mesoporous carbon has been successfully synthesized as non-precious, highly active and durable ORR catalysts by pyrolyzing lysine and melamine in a nitrogen atmosphere using ferric chloride as an activator and SiO_2 nanoparticles as hard templates. The synthesized MNMC is a high

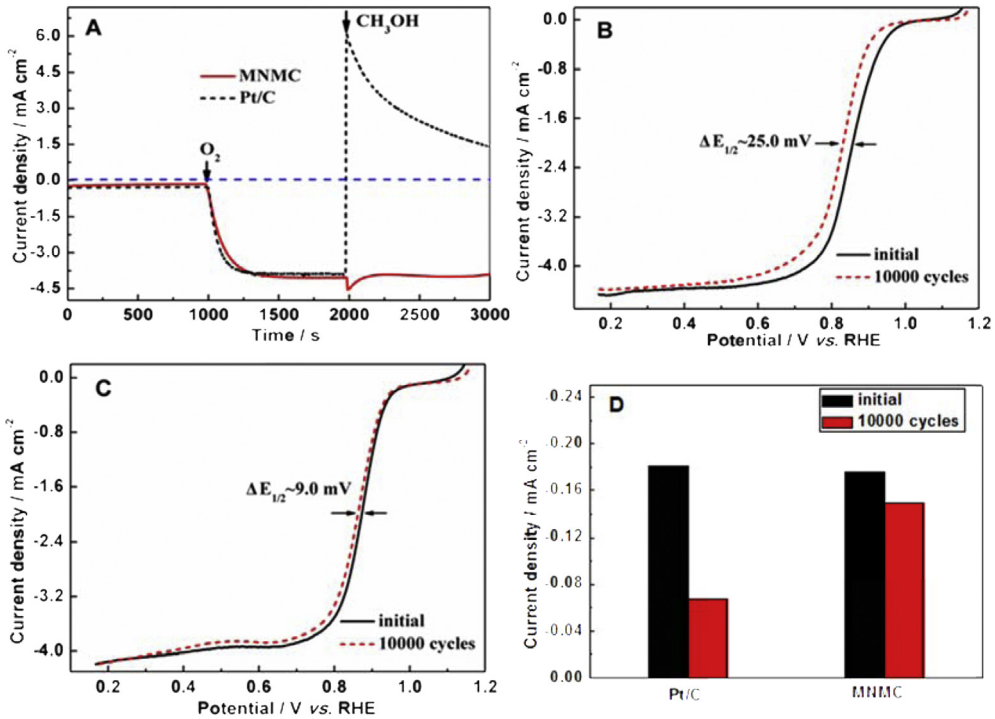

Fig. 7. (A) Current-time chronoamperometric curves of ORR on MNMC and commercial Pt/C at 0.706 V and 1600 rpm in 0.1 mol L^{-1} KOH solution saturated with N_2 (0–1000 s) or O_2 (1000–2000 s) and O_2-saturated 0.1 mol L^{-1} KOH + 3 mol L^{-1} CH_3OH (2000–3000 s) solution. (B and C) LSVs of Pt/C and MNMC before and after 10,000 cycles in O_2-saturated 0.1 mol L^{-1} KOH solution at a scan rate of 5 mV s^{-1} and rotation rate of 1600 rpm, respectively. (D) The current density of Pt/C and MNMC at 0.966 V derived from the data shown in Figure B and C.

surface area material and its BET surface area is measured to be 650 $m^2 g^{-1}$ with PSD in the range of 2.2–34.5 nm. The XPS results reveal that the pyridinic-type N accounts for 40.7% of nitrogen species in MNMC. The LSV results demonstrate that MNMC exhibits higher ORR activity and better stability than commercial Pt/C in alkaline medium, which is efficient, non-precious metal, low cost, and highly active ORR catalyst as a promising alternative of Pt-based catalysts in fuel cells.

Acknowledgments

The authors would like to thank the National Natural Science Foundation of China (21163018, 21363022, and 51362027).

References

[1] S. Wang, D. Yu, L. Dai, D.W. Chang, J.-B. Baek, ACS Nano 5 (2011) 6202–6209.
[2] Z. Chen, D. Higgins, H. Tao, R.S. Hsu, Z. Chen, J. Phys. Chem. C 113 (2009) 21008–21013.
[3] Z.-W. Liu, F. Peng, H.-J. Wang, H. Yu, W.-X. Zheng, J. Yang, Angew. Chem. Int. Ed. 123 (2011) 3315–3319.
[4] Z. Chen, D. Higgins, A. Yu, L. Zhang, J. Zhang, Energy Environ. Sci. 4 (2011) 3167–3192.
[5] S.M. Alia, G. Zhang, D. Kisailus, D. Li, S. Gu, K. Jensen, Y. Yan, Adv. Funct. Mater. 20 (2010) 3742–3746.
[6] P. Balbuena, R. Callejas-Tovar, P. Hirunsit, J. Martínez de la Hoz, Y. Ma, G. Ramírez-Caballero, Top. Catal. 55 (2012) 322–335.
[7] Y. Bing, H. Liu, L. Zhang, D. Ghosh, J. Zhang, Chem. Soc. Rev. 39 (2010) 2184–2202.
[8] S. Liu, H. Zhang, Z. Xu, H. Zhong, H. Jin, Int. J. Hydrogen Energy 37 (2012) 19065–19072.
[9] H. Chen, F. Sun, J. Wang, W. Li, W. Qiao, L. Ling, D. Long, J. Phys. Chem. C 117 (2013) 8318–8328.
[10] L. Qu, Y. Liu, J.-B. Baek, L. Dai, ACS Nano 4 (2010) 1321–1326.
[11] L. Zhang, J. Niu, L. Dai, Z. Xia, Langmuir 28 (2012) 7542–7550.
[12] G. Álvarez, F. Alcaide, P.L. Cabot, M.J. Lázaro, E. Pastor, J. Solla-Gullón, Int. J. Hydrogen Energy 37 (2012) 393–404.
[13] S. Kim, S.-J. Park, Anal. Chim. Acta 619 (2008) 43–48.
[14] X. Cui, F. Cui, Q. He, L. Guo, M. Ruan, J. Shi, Fuel 89 (2010) 372–377.
[15] Y. Deng, Y. Cai, Z. Sun, D. Gu, J. Wei, W. Li, X. Guo, J. Yang, D. Zhao, Adv. Funct. Mater. 20 (2010) 3658–3665.
[16] W. Shen, W. Fan, J. Mater. Chem. A 1 (2013) 999–1013.
[17] M. Seredych, D. Hulicova-Jurcakova, G.Q. Lu, T.J. Bandosz, Carbon 46 (2008) 1475–1488.
[18] Y. Zhao, L. Yang, S. Chen, X. Wang, Y. Ma, Q. Wu, Y. Jiang, W. Qian, Z. Hu, J. Am. Chem. Soc. 135 (2013) 1201–1204.
[19] J.R. Pels, F. Kapteijn, J.A. Moulijn, Q. Zhu, K.M. Thomas, Carbon 33 (1995) 1641–1653.
[20] S. Shanmugam, T. Osaka, Chem. Commun. 47 (2011) 4463–4465.
[21] J.C. Jia, R.F. Wang, H. Wang, S. Ji, J. Key, V. Linkov, K. Shi, Z.Q. Lei, Catal. Commun. 16 (2011) 60–63.
[22] T. Maiyalagan, Appl. Catal. B 80 (2008) 286–295.
[23] Z. Rozlívková, M. Trchová, M. Exnerová, J. Stejskal, Synth. Met. 161 (2011) 1122–1129.
[24] H.-S. Zhai, L. Cao, X.-H. Xia, Chin. Chem. Lett. 24 (2013) 103–106.
[25] T. Zhou, H. Wang, S. Ji, V. Linkov, R. Wang, J. Power Source 248 (2014) 427–433.
[26] H. Wang, H. Da, S. Ji, S. Liao, R. Wang, J. Electrochem. Soc. 160 (2013) H266–H270.
[27] Q.-H. Yang, P.-X. Hou, M. Unno, S. Yamauchi, R. Saito, T. Kyotani, Nano Lett. 5 (2005) 2465–2469.
[28] T. Sharifi, F. Nitze, H.R. Barzegar, C.-W. Tai, M. Mazurkiewicz, A. Malolepszy, L. Stobinski, T. Wågberg, Carbon 50 (2012) 3535–3541.
[29] T. Zhou, H. Wang, K. Julian, S. Ji, V. Linkov, R. Wang, RSC Adv. 3 (2013) 16949–16953.
[30] D. Hulicova-Jurcakova, M. Kodama, S. Shiraishi, H. Hatori, Z.H. Zhu, G.Q. Lu, Adv. Funct. Mater. 19 (2009) 1800–1809.
[31] W. Yang, T.-P. Fellinger, M. Antonietti, J. Am. Chem. Soc. 133 (2010) 206–209.
[32] R. Silva, D. Voiry, M. Chhowalla, T. Asefa, J. Am. Chem. Soc. 135 (2013) 7823–7826.
[33] D. Deng, L. Yu, X. Chen, G. Wang, L. Jin, X. Pan, J. Deng, G. Sun, X. Bao, Angew. Chem. Int. Ed. 52 (2013) 371–375.
[34] J. Liang, Y. Jiao, M. Jaroniec, S.Z. Qiao, Angew. Chem. Int. Ed. 51 (2012) 1–6.
[35] S. Wang , E. Iyyamperumal , A. Roy, Y. Xue, D. Yu, L. Dai, Angew. Chem. Int. Ed. 50 (2011) 11756–11760.
[36] Q. Tang, L. Jiang, J. Qi, Q. Jiang, S. Wang, G. Sun, Appl. Catal. B Environ. 104 (2011) 337–345.